

# *In situ* TEM evaluation of the growth kinetics of Au particles on highly oriented pyrolytic graphite at elevated temperatures

R. Anton and P. Kreutzer

*Institut für Angewandte Physik und Zentrum für Mikrostrukturforschung, Universität Hamburg, Jungiusstraße 11, D-20355 Hamburg, Germany*

(Received 21 July 1999; revised manuscript received 6 January 2000)

Gold particles were vapor deposited onto thin substrates of highly oriented graphite at temperatures from 250 to 350 °C inside a transmission electron microscope. The growth kinetics of individual particles were recorded in real time. Mostly well faceted, flat crystallites grew in epitaxial orientation with (111) faces on top. On substrate areas with low-defect density, particle numbers were in the range of some  $10^9/\text{cm}^2$ , independent of temperature. In highly defective areas, densities were up to  $10^{11}/\text{cm}^2$ . Condensation coefficients were measured in both areas by quantitative x-ray analysis as below 0.01, and around 0.1, respectively, during the early stages of growth. Particle shapes mostly stayed constant during growth, while the projected areas were found to increase in proportion to deposition time. Capture rates of adatoms were determined quantitatively, and compared with calculations on the basis of a diffusion model, leading to a mean adatom diffusion length before desorption of  $5.8 \pm 2.4$  nm on defect free highly oriented pyrolytic graphite at 350 °C. This value corresponds to a difference of the atomic energies of adsorption and diffusion ( $E_a - E_d$ ) =  $0.39 \pm 0.04$  eV.

## I. INTRODUCTION

The kinetics of nucleation and growth of particles on substrates has often been investigated in the past with the aim to obtain more insight in the adatom energetics. Statistical measurements of the rates of particle nucleation and growth may be analyzed on the basis of rate equations for the densities of monomers and clusters. Adequate theories are well developed, for example, by Venables, Spiller, and Hanbücken.<sup>1</sup> One of their main features is that saturation nucleation densities can be expressed in the form of “scaling laws,” with combinations of atomic energies for adsorption  $E_a$ , surface diffusion  $E_d$ , and binding in a cluster as parameters.<sup>2</sup>

In a complementary approach, analysis of particle growth kinetics allows in principle assessment of the adatom diffusion path length  $\lambda$ . This is feasible for the case of incomplete condensation, where  $\lambda$  is limited by the stay time, given by  $E_a$ , and thus correlated to the energy difference  $\Delta E = E_a - E_d$ . In earlier work, we have measured capture rates of individual particles during condensation by *in situ* transmission electron microscopy (TEM) techniques for the case of dendritic growth of gold particles on highly oriented pyrolytic graphite (HOPG) at room temperature.<sup>3</sup> As a result,  $\lambda$  was determined as about 400 nm, corresponding to  $\Delta E = 0.4$  eV. One major aim of the present paper is to investigate whether this value also holds for higher temperatures, at which particles do not grow dendritic, but in the form of well faceted, more three-dimensional crystallites.<sup>4</sup> The main difference to the case of dendritic growth is that, at the early stages, the sizes of the adatom capture areas are expected to be much smaller than the general interparticle distances, as the adatom lifetime on the substrate will be strongly reduced at elevated temperatures. Also, the particles assume more three-dimensional shapes, and this influences the ratio of the capture rates by diffusion and direct impingement.

## II. EXPERIMENTAL PROCEDURES

Vapor depositions of gold on graphite substrates were performed in a transmission electron microscope (Philips EM400), which had been modified for *in situ* experimentation. Details of the apparatus and specimen preparation have been described in earlier papers.<sup>3,5</sup> Prior to the depositions, substrates were heated to 600 °C for several hours to remove any contamination from the surface. Depositions were performed at temperatures ranging from 250 to 350 °C. The vapor beam flux was monitored with a quadrupole mass spectrometer. During deposition experiments, the residual gas pressure was in the range of  $1 - 2 \times 10^{-8}$  mbar with the cold trap at liquid nitrogen temperature. Virtually no hydrocarbons could be detected with the mass spectrometer. Particle nucleation and growth was imaged via a closed circuit TV chain, and was recorded on video tape. By using an electronic image intensifier, and not too high magnifications, the electron beam density on the specimen could be kept below  $1 \text{ A}/\text{cm}^2$ , which is about one order of magnitude lower than needed for normal imaging. In fact, at elevated substrate temperatures, no indications of electron beam induced artifacts were observed when comparing irradiated and nonirradiated areas during and after growth of particles.

After deposition, specimens were transferred to another TEM with x-ray analysis facilities (EDX). Measurements of the  $L$  emission of Au allowed us to estimate the masses of individual particles. Calibration of the x-ray signal was possible by means of some particles with well-defined shapes, in particular decahedra with fivefold symmetry (multiply twinned particles) and other, obviously three-dimensional aggregates (see Sec. III C).

## III. RESULTS

### A. General observations

At temperatures at and above 250 °C, Au particles mostly grow with well-faceted shapes, exhibiting mainly (111) and

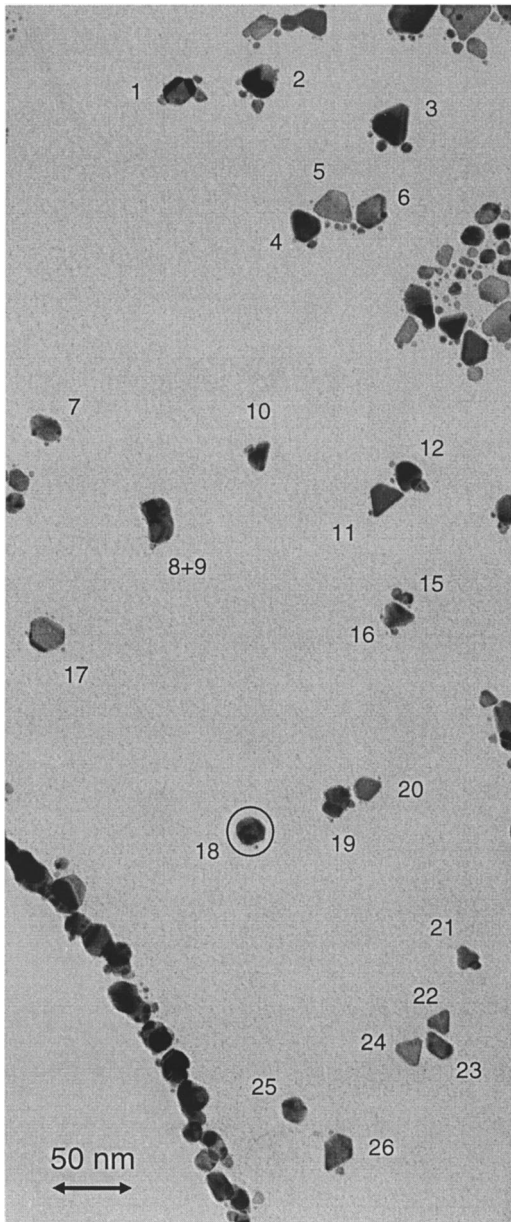


FIG. 1. TEM image, showing Au particles deposited on HOPG at 350 °C in an area with low-defect density. A patch with high-defect density is seen at the upper right, while a step bunch is decorated at the lower left. The area with numbered particles was also imaged during deposition. Part of this is shown in Fig. 2. Note several flat, faceted crystallites, as well as more rounded or irregularly shaped particles. Particle #25 is a decahedron. Note also secondary nucleation in the vicinity of larger particles. The circle around particle #18 is drawn to illustrate the assumed size of an adatom capture zone of width  $\lambda$  (see Sec. IV).

(100) surfaces. This is consistent with early results of Wayman and Darby, who observed a transition from dendritic to faceted growth on vacuum cleaved graphite at above 100 °C.<sup>6</sup> *In situ* observations during growth revealed that such more three-dimensional shapes not only persisted from the beginning, but also developed after coalescence events. Figure 1 shows an area of a HOPG substrate with Au particles deposited at 350 °C. This image was taken on film after the end of deposition. A series of video images of part of this area, taken during growth, is collected in Fig. 2. Two sorts of

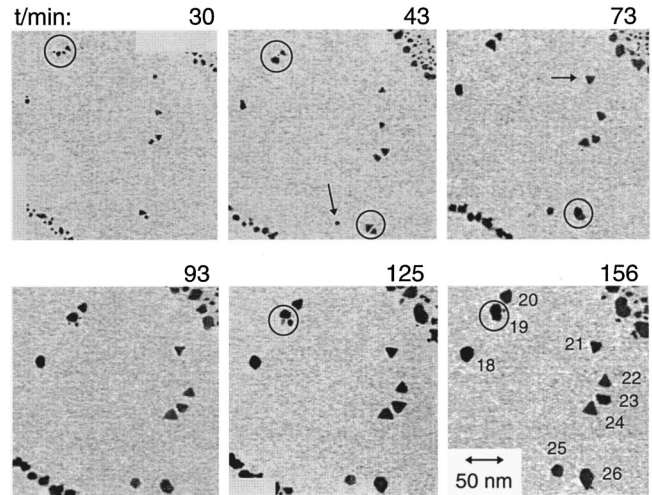


FIG. 2. Series of video images taken during growth of Au particles shown in Fig. 1 (lower part). Several coalescence events are marked with circles. Coalescence does generally not lead to bulk 3D recrystallization. Arrow at  $t=43$  min indicates first appearance of particle #25, which maintained decahedral shape during growth. Arrow at  $t=73$  min indicates flip over of particle #21.

particles can be discerned, namely, single crystalline, flat ones exhibiting mainly (111) and (100) facets, as for example particles #3, #4, #6, #17, and #22 through #24, and more rounded or irregularly shaped ones, showing internal variations of Bragg contrast, like #1, #2, #10, #18, #19, and #25. These are not single crystals, and generally appear to be more three dimensional than the faceted particles. This is supported by x-ray measurements discussed below.

In the area depicted in Fig. 1, the particle number density exhibits a rather low value of about  $3 \times 10^9/\text{cm}^2$ , while much higher densities were often found elsewhere, with sharp borders to the low-density areas. Similar variations have been observed in the case of depositions at room temperature, as reported earlier, and are deemed to be caused by inhomogeneous distributions of defects on the substrate surface, which are decorated by the nucleation of Au particles. Indications are that even the areas with low-particle number densities are not free of defects, since about the same population density as stated above was also measured at lower temperatures, e.g., at 300 °C, and even at room temperature.<sup>3</sup> For purely statistical nucleation, a strong dependence on temperature would be expected.

Most particles grow epitaxially oriented with  $(111)_{\text{Au}} \parallel (0001)_{\text{graphite}}$  and  $[112]_{\text{Au}} \parallel [2110]_{\text{graphite}}$ , as was detected by electron diffraction. Deviations from the exact azimuthal orientation by several degrees are quite common, indicating that the binding of the particles to the substrate is not very strong. This is also supported by the observation of significant displacements of particles during growth, possibly induced by charging. Such movements can be seen in Figs. 2 and 3. The latter shows a superposition of contour lines, drawn at various stages during the growth of several neighboring particles. Obviously, particles can move as such, and apparent displacements do not simply result from anisotropic growth in preferred directions.

Coalescence of neighboring particles often produced intermediate, irregularly shaped aggregates, which subsequently developed into well-faceted crystallites, as for ex-

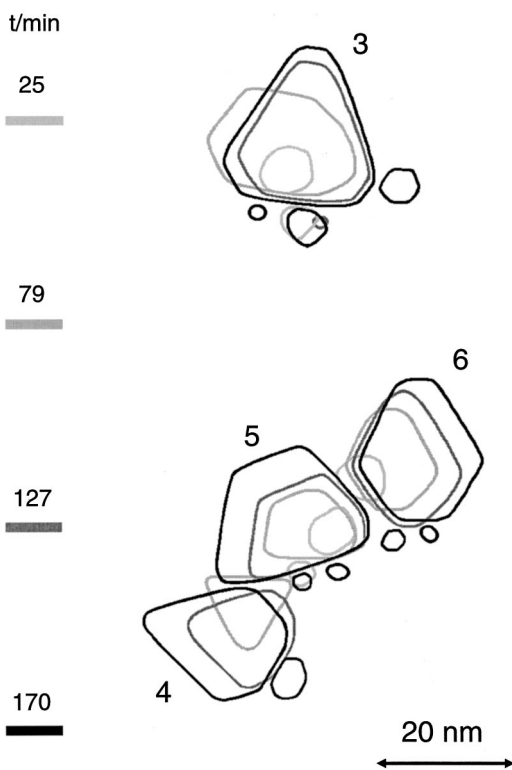


FIG. 3. Superposition of contour lines of the area with particles #3 to #6 as in Fig. 1, drawn at about equal time steps as indicated. This illustrates displacements and rotation of whole particles (#4 and #6), quasi-2D recrystallization after coalescence (particle #3), development of (111) and (100) side facets, and secondary nucleation.

ample, particle #3 after  $t=55$  min, #5 after  $t=25$  min, or #26 after  $t=73$  min. Coalescence did not always result in three-dimensional recrystallization. As an example, another group of particles merged into particle #19 at  $t=130$  min, which appears polycrystalline, and its projected area, just after coalescence, is about the sum of the original particles. The coalescence of particles #8 and #9 represents a similar case. In general, indications are that all particles have more or less flattened shapes, with heights being significantly smaller than widths. More accurate estimates will be given in the discussion of x-ray measurements in Sec. C.

### B. Particle growth rates

Figures 4(a) and 4(b) show representative examples for the increase of the projected particle areas with deposition time. Taking into account the scatter of the data, which is mainly caused by the limited contrast in the video images, the growth rate of any one particle appears approximately constant during growth, except during coalescence. Several such events are marked with arrows in Figs. 4(a) and 4(b). Subsequent lateral growth was mostly found to proceed with about similar speed as before. Nucleation of satellite particles at distances of a few nm did virtually not cause a reduction of the growth rate, as might be expected, due to competitive capture. See, for example, particles #3, #5, and #6. Especially interesting is the case of #5, which is partly embraced by particles #4 and #6, but grows even slightly faster than the latter two. This may be caused by a somewhat

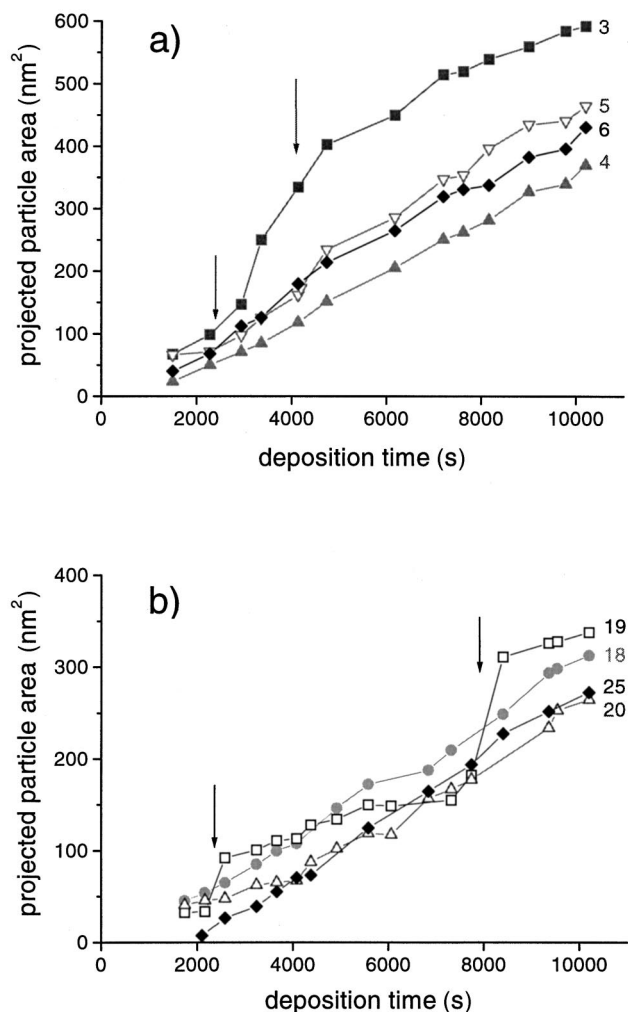


FIG. 4. (a) Plot of the projected areas of flat, faceted particles #3 to #6 vs deposition time. Experimental conditions as in Fig. 1. Arrows indicate coalescence events of particle #3. The presence of particles #4 and #6 does not seem to markedly influence the growth speed of particle #5, which is closely located in between. (b). same for particles #18 (rounded shape, “3D”), #19 (irregular shape after coalescence), #20 (triangular shape), and #25 (decahedron).

smaller thickness, as is indicated by its relatively low contrast, especially when compared with particle #4. A similar behavior is observed for the group of particles #23, #22, and #24. These observations clearly show that shadowing of the diffusion flux does not significantly influence the particle growth rate. Apparently, the adatom diffusion length on the substrate is rather limited, and direct impingement is not negligible, even for small particle sizes. This corresponds to the fact that no correlation of the particle growth rate with the size of the surrounding area was found, in contrast to the case of dendritic growth at room temperature, where the capture areas are limited by the competition of neighboring aggregates.<sup>3</sup>

### C. X-ray measurements

Quantification of capture rates requires knowledge of the volume of the particles, which is usually not provided by TEM images alone. We have tried to obtain estimates of the three-dimensional shapes from measurements of the x-ray

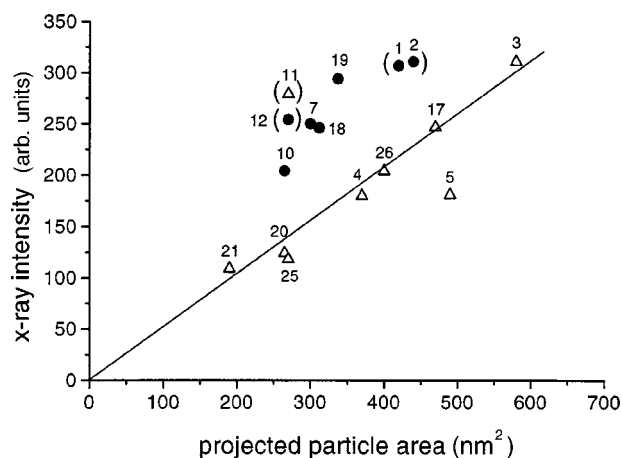


FIG. 5. Plot of the x-ray yield of a number of particles vs their projected areas. Open triangles denote flat, faceted crystallites, solid circles more rounded, 3D particles. Particles #1 and #2 exhibit irregular shapes, as is suggested by internal Bragg contrast, seen in Fig. 1. The straight line is a guideline to the eyes, which indicates virtually similar heights of most of the flat crystallites.

yields of individual particles by EDX, and by correlations with their projected areas. It should be noted that not all particles are taken into account for the following considerations, in particular those with large satellite particles, of which the individual x-ray yields could not be determined. In Fig. 5, the Au-L intensity is plotted vs the projected area of individual particles. Two classes of particles can be discerned. The intensities from the apparently flat, well-faceted crystallites are generally lower than those from the more three-dimensional aggregates, at similar lateral sizes. Obviously, the latter are thicker than the flat ones. Interestingly, the data from the flat crystallites suggest a proportional relationship with the projected area, which means that their heights are about equal. Only particle #5 exhibits a somewhat too low x-ray yield, indicating a reduced thickness. In fact, this was already indicated by the lower contrast in the TEM image.

Calibration of the x-ray yield with respect to volume was tried by means of a few multiply twinned particles with decahedral shape, like #25 visible in Figs. 1 and 2. Such particles are frequently found to nucleate at higher temperatures also on other substrates, even on amorphous carbon.<sup>7</sup> While the volume of an ideal decahedron can be calculated from the projected area, the question arises, whether the interface at the substrate is truncated, which may be caused by lowering of the interfacial energy with respect to the surface energy. However, there are indications that this is not significant here. According to the Wulff-Kaichew construction, the degree of truncation is given by the ratio of the adhesion energy and the surface energy of the metal. In fact, the adhesion of gold particles to the graphite substrate seems to be rather low, as was discussed above. Also, the binding energy of gold atoms to graphite is much lower than to each other. Moreover, detailed TEM studies of the shapes of supported decahedral and icosahedral gold particles, for example by Heinemann *et al.*,<sup>8</sup> did not indicate truncations, which should be detectable, for example, by distortions of thickness fringes in weak beam dark field images. Clearly, any truncation of a decahedron in fivefold orientation could not exceed

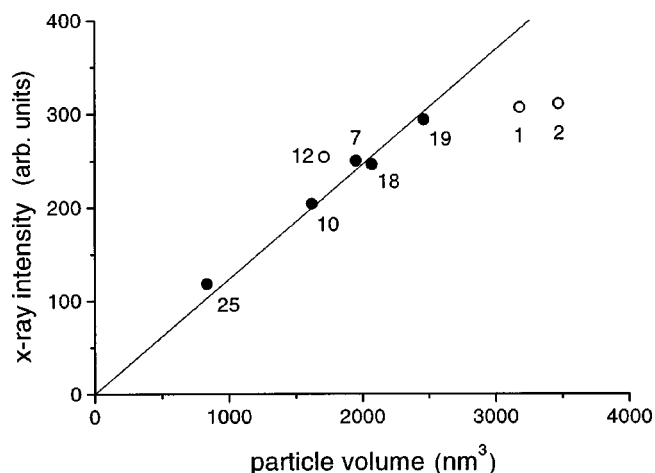


FIG. 6. Plot of the x-ray yield of selected particles vs their volume. The straight line is a calibration curve, calculated on the basis of the volume of particle #25, which is a decahedron. Volumes of the other particles are estimated by assuming half-spherical shapes. This approximation seems to be justified for particles #7, #18, and possibly #19, but not for particles #1, #2, and #12, due to more quasi-2D or more bulky shapes, respectively.

half of the particle height, at a given lateral size. For the above reasons, we believe it is much less, if present at all. In any case, an error in calculating the particle volume would affect the deduced adatom walk length correspondingly. However, we will see below that the maximum possible error of 50% would alter the calculated activation energy only marginally. A further discussion follows in Sec. IV below.

In Fig. 6, the x-ray intensities of selected particles are plotted vs their estimated volume. The straight line represents the calibration with particle #25 under the assumption of an ideal decahedral shape. If we assume averaged half spherical shapes for particles #7, #10, #18, and #19, which appear somewhat bulky or irregular in the TEM image, their volumes, as calculated from the projected areas, would fit the calibration reasonably well. From the calibration in Fig. 6, the heights of the flat crystallites, as depicted in Fig. 5, are calculated to about  $4.1 \pm 0.3$  nm (see Table I below), whereas the height of particle #5 (3.3 nm) is considerably lower, as expected. If the calibration particle #25 would be truncated, these heights would be correspondingly reduced.

Quantitative x-ray measurements of the particle masses allowed us to calculate the condensation coefficient, integrated up to the end of deposition at  $t = 10\ 200$  s. As a result, at a substrate coverage of the order of 1%, a fraction of only about 0.001 of the flux of Au from the vapor beam was present in the areas with low-particle number densities, like that shown in Fig. 1. In the high-population areas, at a coverage of roughly 50%, the integrated condensation coefficient was still below 0.05. For comparison, a value of  $0.3 \pm 0.2$  was estimated for the case of dendritic growth at room temperature, under otherwise similar conditions, at a substrate coverage of only 5%, quickly approaching unity, after less than 3000 s of deposition with similar flux!<sup>2</sup>

#### IV. DISCUSSION

Our *in situ* TEM deposition experiments and x-ray measurements clearly revealed that the condensation of Au on

HOPG is initially extremely incomplete at elevated temperatures, given by a very short adatom stay time  $\tau$  and walking distance  $\lambda$  on the substrate before desorption. These quantities are related to the atomic energies for adsorption  $E_a$ , and surface diffusion  $E_d$ , by

$$\tau = \nu_a^{-1} \exp\left\{\frac{E_a}{kT}\right\}, \quad (1)$$

where  $\nu_a$  is the attempt frequency for desorption, and

$$\lambda = \frac{a}{2} \sqrt{\frac{\nu_d}{\nu_a}} \exp\left\{\frac{E_a - E_d}{2kT}\right\}, \quad (2)$$

where  $a$  is the single jump distance, and  $\nu_d$  is the attempt frequency. Although the latter is expected to be a little smaller than  $\nu_a$  here we approximate their ratio as unity. While the adatom stay time cannot be deduced from the particle growth kinetics alone, the mean walking distance can be assessed from measurements of the capture rates on the basis of a suitable diffusion model. In our previous work, we have determined  $\lambda$  for Au on HOPG at room temperature to be about 400 nm, resulting in  $E_a - E_d = 0.40$  eV, with an error margin of 0.05 eV.<sup>2</sup> Arthur and Cho have found from atomic scattering experiments with Au on natural graphite that even at room temperature, condensation is initially incomplete, and given an upper limit for  $\tau$  of 10 ms.<sup>9</sup> This value corresponds to an upper limit for  $E_a$  of 0.64 eV, for  $\nu_a = 10^{13}$  s, and would fix  $E_d$  to 0.24 eV. Extrapolation to say 300 °C would result in an adatom stay time of some  $10^{-8}$  s, and in a diffusion length of below 10 nm. The aim of our present work is to investigate, whether such an estimate would also explain the growth kinetics of more compact, small crystallites at higher temperatures, e.g., at rather different boundary conditions for adatom diffusion and capture than for dendritic growth at room temperature.

For the latter case, we argued that rapid lateral growth is predominantly fed by capture of adatoms diffusing on the surrounding substrate surface. Direct impingement contributes only at late stages, and mainly to growth in height, due to the existence of a diffusion barrier (Ehrlich-Schwoebel barrier) at the particle edges. In contrast, for the present case of nucleation and growth of more compact particles at elevated temperatures, the contribution of direct impingement is expected to become significant much earlier, because of the considerably reduced capture zone for diffusing adatoms.

The following discussion is based on the same diffusion model as discussed in our earlier paper, only the boundary conditions are changed. A growing particle (mean radius  $R$ ) is a sink for adatom diffusion, and the capture rate  $\Phi(R)$  is obtained by integrating the capture probability over the surroundings up to a certain radius  $r_s$ . In contrast to the case of dendritic growth at room temperature, this is not limited here by competitive capture by neighboring aggregates. Assuming the usual profile of the adatom capture probability, expressed by the ratio of Bessel functions, 67 % of the adatoms are captured from an annulus with  $r_s = \lambda$ . We take  $r_s = 10\lambda$ , which leaves an escape probability of less than 1 %. In any case,  $\lambda$  is expected to be so small that during the early stages, competitive capture will generally not be significant.

For comparison with experiment, the particle mean radius  $R$  has to be expressed as function of deposition time, and is

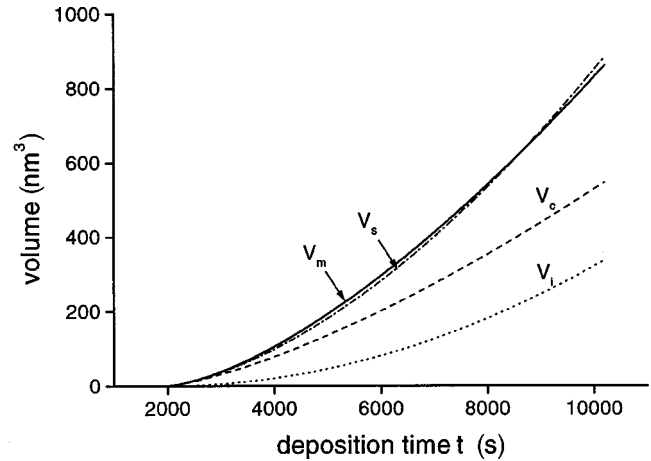


FIG. 7. Increase of the volume of particle #25 (decahedron), as well as of the contributions of capture and direct impingement vs deposition time. The solid curve ( $V_m$ ) represents the volume as calculated from the measured projected area. The dash-dotted curve ( $V_s$ ) is the sum of the contributions of direct impingement (dotted  $V_i$ ), and capture (dashed  $V_c$ ).  $V_s$  was calculated to fit  $V_m$  by adjusting the adatom diffusion length  $\lambda$  to 3.9 nm.

calculated from the measured lateral growth rate. The increase with time  $t$  of the particle volume by capture is calculated by integrating  $\Phi(R)$  over time starting with nucleation at  $t = t_0$ . Similarly, the accumulated contribution of direct impingement is obtained by integrating the adatom flux times the projected area over time as above. Here, we imply that condensation of metal on metal is complete under our conditions.

Calculations were feasible for a number of particles with virtually constant shape during growth, allowing us to estimate the variation with time of their total volume. This data were fitted by calculating the contributions of capture and direct impingement as explained above. As an only fit parameter, the adatom walk distance  $\lambda$  was suitably adjusted. This is illustrated in Fig. 7 for the example of the pentagonal particle #25. A best fit was obtained with  $\lambda = 3.9$  nm, corresponding to a difference of the energy parameters of  $\Delta E = E_a - E_d = 0.35$  eV, when assuming a jump length  $a$  of 0.3 nm. If the particle were truncated by 50 % at maximum,  $\lambda$  would be reduced to roughly 1.5 nm, and  $\Delta E$  would be reduced by about 0.1 eV. However, we estimate that the error is much smaller, as was already discussed above. A further argument against significant truncation arises here, in that no good fit of the slope of the measured increase of the volume with time could be obtained. This is due to the altered time dependence of the ratio of direct impingement to capture. The latter would be reduced, but direct impingement would not.

It is apparent that the integrated, relative contribution of direct impingement strongly increases with time, and amounts to more than 30 % at the end of deposition, when the particle diameter reached about 24 nm. In contrast, for dendritic growth at room temperature, such a fraction of direct impingement was only assumed at a particle diameter of some hundreds of nm, due to the much greater capture rate.<sup>2</sup>

The variation with time of the volume of the faceted, flat particles was estimated by assuming growth in height according to a power law  $h(t) = h_0 + \beta(t - t_0)^n$ . Taking into

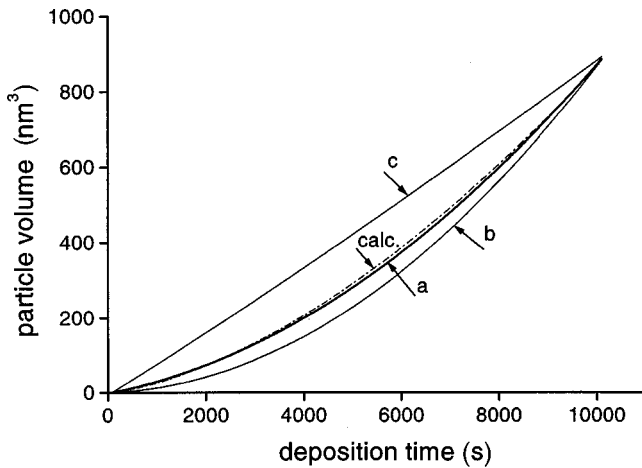


FIG. 8. Increase of the volume of the flat, faceted particle #21 with deposition time. The thick solid curve (a) is calculated from the measured projected area with the assumption of linear growth in height from 1.3 to 4.3 nm, so as to approach the volume measured by EDX at the end of deposition. The thin, solid curves (b and c) are calculated by assuming initial heights of 0.3 and 4.0 nm, respectively. The dash-dotted curve was calculated from the contributions of direct impingement and capture, so as to fit curve a by adjusting  $\lambda$  to 4.2 nm. Curves b and c could not be fitted (see text).

account the measured constant growth rate of the projected area, the variation with time of the volume would then be given by the volume at the end of deposition. Several attempts were made to fit these curves by suitably adjusting the initial height  $h_0$ , assumed shortly after nucleation, the growth rate in height  $\beta$ , as well as the power  $n$ . As an example, results for particle #21 are plotted in Fig. 8. A best fit was obtained with  $n=1$ ,  $h_0=1.3$  nm,  $\beta=0.00031$  nm/s, and with  $\lambda=4.3$  nm (curve a in Fig. 8). In fact, linear growth in height appears reasonable, although good fits were also possible with  $0.5 < n < 1$  and  $0.3 < h_0 < 1.3$  nm. A power  $n < 1$  would mean initially fast vertical growth, slowing down subsequently. In any case, for parameters within the above regimes, variations of  $\lambda$  were less than 0.2 nm. On the other hand, the (not reasonable) assumption of virtually constant height during growth, as was found for dendritic growth at room temperature, resulted in significant deviations of the slopes of the curves, which could not be compensated by adjusting  $\lambda$  (curve c in Fig. 8). Interestingly, very similar sets of parameters were also found as best fits for the growth curves for most of the other flat particles, suggesting initial heights of the order of 1 nm. It is clear that these flat crystallites are kinetic forms, whereas the equilibrium shape would be near to a sphere, with (111) and (100) facets.<sup>10</sup> The evolution of particle forms during condensation has been addressed by Bermond and Venables.<sup>11</sup> It is argued that growth on atomically flat surfaces may be hindered by the lack of nucleation sites, e.g., kink sites or defects. This would lead to quasi-two-dimensional growth. In our case, direct impingement contributes significantly to growth at later stages, obviously without leading to pronounced two-dimensional (2D) growth. Thus, it appears reasonable that adatom diffusion from the top surface down the edges is slow, at least. It is interesting to compare this behavior with the case of dendritic growth of very flat aggregates, where we have con-

TABLE I. Geometrical data and atomic diffusion length for a number of particles deposited on HOPG at 350 °C. Volume data are based on the calibration of particle #25, assuming an ideal decahedral shape (see text). Height values are calculated by dividing volume by area. Height values of parentheses refer to average values. \* indicates assumed, average shapes.

Particle no.	Projected area/nm <sup>2</sup>	Volume /nm <sup>3</sup>	Height /nm	Diffusion length /nm	Particle shape
3	593	2527	4.3	4.8	faceted, flat
4	367	1500	3.9	5.2	faceted, flat
5	465	1530	3.3	4.8	faceted, flat
7	312	2070	(6.6)	8.2	half-sphere*
10	265	1622	(6.1)	8.7	irregular
17	486	1966	4.0	5.9	faceted, flat
18	311	2060	(6.6)	8.9	half-sphere*
20	253	993	3.9	4.5	faceted, flat
21	208	903	4.3	4.2	faceted, flat
25	279	862	(3.1)	3.9	decahedron
26	413	1662	4.0	4.5	faceted, flat

cluded that crossing from the top surface down the edge and vice versa would be hindered by the existence of an Ehrlich-Schwoebel barrier.<sup>3</sup> At elevated temperatures, however, this effect may be significantly reduced. In fact, assuming an activation energy for diffusion on the (111) surface of 0.2 eV, an additional barrier of 0.1 eV, for example, would reduce the diffusion flux by a factor of 1/50 at room temperature, but only of 1/6 at 350 °C. Nevertheless, this would not be negligible.

For some of the bulky particles, in particular #7 and #18, the approximation of roughly half-spherical habits would explain their volume as determined from x-ray measurements. For all particles with reasonably calibrated volumes, and which did not experience coalescence during growth, an individual adatom diffusion length  $\lambda$  was obtained as a fit parameter for the growth kinetics. In Table I, these values are listed together with geometrical data as projected area, volume, and (average) height after deposition. Despite some scatter, the adatom growth lengths  $\lambda$  are all of the same order. Taking only the decahedron and the flat crystallites, a mean value of  $4.7 \pm 0.6$  nm is calculated on the basis of our suggested calibration. Using Eq. (2), the mean value of the energy difference  $\Delta E = E_a - E_d$  is then calculated to  $0.37 \pm 0.02$  eV, taking the jump length  $a=0.3$  nm. Allowing a (not reasonable) truncation of the calibration particle of 50% would reduce the average  $\lambda$  to about 2.6 nm, resulting in  $\Delta E=0.31$  eV. On the other hand, the more bulky particles produce somewhat increased values for reasons not yet understood, resulting in a total average for all particles of  $\lambda=5.8$  nm, which would yield  $\Delta E=0.39$  eV. Thus, the maximum error in  $\Delta E$  is certainly smaller than 0.08 eV, and probably much less.

## V. CONCLUSION

Our *in situ* TEM investigations of the growth kinetics of small gold crystallites on HOPG at elevated temperatures were intended to complement our earlier work on dendritic growth at room temperature.<sup>3</sup> The aim was to check whether

the very different growth modes can be described with the same model of adatom diffusion and capture. It turned out that evaluation of nucleation densities was not feasible, as no dependence on temperature was found. Therefore, we believe that nucleation takes place at defect sites, which, however, are inhomogeneously distributed on the substrate surface. On the other hand, the initial condensation coefficient was measured by quantitative EDX to below  $10^{-3}$ , which indicates that binding to these sites is not very strong and/or their distances are much greater than the mean adatom walk distance.

Epitaxial particles grew well faceted, with flat, (111) top surfaces, and assumed more or less similar heights, as was concluded from EDX measurements of their volumes. In general, particle growth kinetics could be modeled by calculating the contributions of capture and of direct impingement. The latter was given by the deposition rate, and by the measured growth rate of the projected areas. The capture zones are limited by adatom diffusion length before desorption  $\lambda$ . Fitting calculations were especially feasible for particles with known and constant shape during growth, e.g., decahedra, and for most of the flat, epitaxial particles exhibiting virtually constant growth rates of the projected areas. As an average over all particles,  $\lambda$  was determined to about 5.8 nm, corresponding to an energy difference  $E_a - E_d = 0.39$  eV, with an estimated error of the order of  $\pm 0.04$  eV. This value agrees remarkably well with the result of 0.40 ( $\pm 0.05$ ) eV obtained from our earlier analysis of dendritic

growth at room temperature, where the walk distance of the order of several hundred nm leads to pronounced quasi-2D growth, and the contribution of direct impingement becomes only significant for rather large particles. At about 350 °C, however, with  $\lambda$  being two orders of magnitude lower, the relative contribution of capture, although being dominant initially, strongly decreases with growing particle size. Furthermore, our fit calculations revealed that the height of the flat, faceted crystallites is not constant, rather growth proceeds in three dimensions, starting with initial heights between roughly 0.3 nm and 1.5 nm. It is clear that these growth forms are determined by kinetics and not by equilibrium. This raises the question as to the role of an Ehrlich-Schwoebel type barrier at the edges. For the case of dendritic growth at room temperature, it was argued that such a barrier causes lateral growth being mainly fed by capture, and vertical growth by direct impingement.<sup>3</sup> For the present case of growth at higher temperatures, this effect is expected to be reduced, and a clear separation can not be made. However, the large contribution of direct impingement indicates that the probability of adatoms jumping down from the top surface is at least limited.

#### ACKNOWLEDGMENT

Thanks are due to the Volkswagenstiftung for support of part of this work.

<sup>1</sup>J. A. Venables, G. D. T. Spiller, and M. Hanbücken, Rep. Prog. Phys. **47**, 399 (1984); J. A. Venables, Surf. Sci. **299/300**, 798 (1994).

<sup>2</sup>H. Brune, Surf. Sci. Rep. **31**, 121 (1998).

<sup>3</sup>R. Anton and I. Schneiderit, Phys. Rev. B **58**, 13 874 (1998).

<sup>4</sup>C. R. Henry, Surf. Sci. Rep. **31**, 231 (1998).

<sup>5</sup>R. Anton and M. Harsdorff, Vak.-Tech. **34**, 39 (1985); R. Anton, O. Reetz, and A. A. Schmidt, Ultramicroscopy **41**, 303 (1992).

<sup>6</sup>C. M. Wayman and T. P. Darby, J. Cryst. Growth **28**, 53 (1975).

<sup>7</sup>See, for example, H. Hofmeister, Cryst. Res. Technol. **33**, 3 (1998).

<sup>8</sup>K. Heinemann, M. J. Yacaman, C. Y. Yang, and H. Poppa, J. Cryst. Growth **47**, 177 (1979).

<sup>9</sup>J. R. Arthur and A. Y. Cho, Surf. Sci. **36**, 641 (1973).

<sup>10</sup>J. C. Heyraud and J. J. Métois, Acta Metall. **28**, 1789 (1980).

<sup>11</sup>J. M. Bermond and J. A. Venables, J. Cryst. Growth **64**, 239 (1983).